International Journal of Innovative Environmental Studies Research 14(2):238-254, April-June, 2026

© SEAHI PUBLICATIONS, 2026 www.seahipublications.org ISSN: 2354-2918

DOI:10.5281/zenodo.21208258

Copper-Modified Snail Shell Biochar For Optimised Metronidazole Removal Via Rsm And Adsorption Modelling

Udowa Emily Omotekoro [1], Egbuchunam Theresa O. [2], Mbonu I. J.[3], Ovuoraye Prosper Eguono[4]

[1]Department of Chemistry, College of Education, Warri, Nigeria

[2]Department of Chemistry, Federal University of Petroleum Resources, Effurun, Nigeria

[3] Department of Chemistry, Federal University of Petroleum Resources, Effurun, Nigeria

[4]Department of Chemical Engineering, Federal University of Petroleum Resources, Effurun, Nigeria

[1]Udowa.emily@coewarri.edu.ng
[2]Egbuchunam.theresa@fupre.edu.ng
[3] Mbonu.idongesit@fupre.edu.ng
[4] Ovuoraye.prosper@fupre.edu.ng

ABSTRACT

Metronidazole, a widely used antibiotic, persists in aquatic environments and poses risks to ecosystems and public health. Lowcost agricultural waste derived adsorbents offer a sustainable alternative to conventional water treatment technologies. This study investigates the adsorption of metronidazole onto copper modified snail shell biochar (Cu-SSB) using response surface methodology to identify optimal removal conditions. Shells of Lissachatina fulica were pyrolysed at 700°C and impregnated with 0.5 M $CuSO_4$ to produce Cu-SSB, characterised by SEM-EDX, XRD, FTIR, and BET analysis. A Central Composite Design (30 runs) optimised four variables: pH (3–10), dosage (10–50 mg), contact time (20–120 min), and initial MDZ concentration (30–100 mg/L). Kinetic and isotherm data were fitted by nonlinear regression to PFO, PSO, Elovich, Langmuir, Freundlich, and Temkin models. Characterisation confirmed successful copper incorporation, with a high BET surface area of 348.71 m^2/g, crystalline CuO phases verified by XRD, and a point of zero charge at pH 8.53. The RSM reduced quadratic model ($R^2 = 0.8910$, $p < 0.0001$) identified optimal conditions at dosage 39.53 mg, contact time 35.09 min, and initial concentration 30.34 mg/L, yielding 99% MDZ removal. Equilibrium data best fitted the Langmuir model ($R^2 = 0.9823$, $q_m = 11.93$ mg/g), indicating monolayer adsorption, while pseudo-first-order kinetics provided the strongest fit ($R^2 = 0.8320$), suggesting surface-site-controlled uptake. Cu-SSB is a highly effective, low-cost adsorbent for metronidazole removal, with RSM-optimised conditions achieving near-complete elimination from water.

Keywords: Adsorption, Biochar, Metronidazole, Response Surface Methodology, Water Treatment

INTRODUCTION

Metronidazole (MDZ) is a broad-spectrum antimicrobial used to treat bacterial and protozoal infections, and it has turned up with increasing frequency in rivers, lakes, and groundwater worldwide (Ighalo et al., 2020; Abdi et al., 2025). Hospital wastewater is one of the main entry routes. MDZ has been detected in effluents from hospitals in India and Iran, with antibiotic concentrations reaching as high as 236.6 µg/L in some samples; another study found MDZ in all 15 hospitals surveyed and linked several of those discharges to measurable ecological risk for green algae (Diwan et al., 2009; Majidi et

al., 2024). Ecotoxicity data support that concern even low chronic exposure affects freshwater algae (Lanzky & Halling-Sørensen, 1997).

The issue is compounded by the fact that standard treatment infrastructure was not designed for this class of pollutant. Primary and secondary wastewater treatment plants do not efficiently remove pharmaceutical residues, which has pushed researchers toward tertiary interventions (Sophia & Lima, 2018). Advanced oxidation, adsorption, and membrane separation have all been proposed for MDZ specifically, but each carries practical constraints that limit full-scale uptake (Ighalo et al., 2020; Abdi et al., 2025). Among these options, adsorption stands out for its operational simplicity, cost-effectiveness, and reliable performance at low pollutant concentrations. Biochar has attracted considerable attention as an adsorption platform for antibiotics because it is renewable, inexpensive, and responsive to surface modification (Sophia & Lima, 2018; Sen et al., 2023; Jia et al., 2024). Recent work on MDZ specifically is encouraging. Polymer-modified almond-shell biochars achieved removal efficiencies between 92.42% and 97.44% depending on the modification route, while pine-cone biochar removed 98.57% of MDZ under optimised conditions (Ren et al., 2025; Chebbi et al., 2023). These results show that the performance ceiling for waste-derived biochars is high when the surface chemistry is properly engineered.

Shell-derived feedstocks are worth particular attention because their carbonate-rich composition gives them a distinct surface chemistry after pyrolysis. In one lobster-shell study, the dominant inorganic phase in the resulting biochar was $CaCO_3$, and polyethyleneimine modification introduced amine groups that substantially improved Cu(II) uptake (Jiang et al., 2022). That same study applied Box-Behnken response surface design to optimise concentration, pH, and dose simultaneously, demonstrating how multivariable experimental design captures interaction effects that one-factor-at-a-time testing misses (Jiang et al., 2022). Copper-modified snail-shell biochar applied to MDZ removal remains largely unexplored, but the shell-biochar literature makes it a rational next step. Copper impregnation is a reasonable modification strategy for this system. Post-synthesis metal loading consistently increases active site density, shifts surface charge behaviour, and opens stronger interaction pathways for target molecules — in several biochar systems it has transformed a moderate adsorbent into a much more effective one (Sen et al., 2023; Jia et al., 2024). For snail-shell biochar, copper impregnation should raise reactivity and binding heterogeneity relative to the unmodified material, which translates directly to better MDZ uptake.

Given that adsorption performance depends on pH, adsorbent dose, contact time, and initial contaminant concentration — and that these variables interact — Response Surface Methodology (RSM) is a more efficient optimisation tool than sequential single-variable testing. RSM estimates main effects and interaction terms simultaneously while keeping the number of experimental runs manageable. The lobster-shell study illustrates the point: Box-Behnken design identified near-optimal Cu(II) removal conditions and quantified which variables mattered most, in far fewer runs than a full factorial design would have required (Jiang et al., 2022). This study therefore prepares copper-modified snail-shell biochar (Cu-SSB), evaluates its MDZ adsorption performance, optimises process conditions using RSM, and interprets the underlying adsorption behaviour through isotherm and kinetic modelling. The goal is to produce a low-cost adsorbent from locally available waste material and generate mechanistic data that can support scale-up and future regeneration work — filling a clear gap between the growing MDZ adsorption literature and the limited body of work on copper-modified shell-derived biochars.

2. MATERIALS AND METHODS

2.1 Materials

Metronidazole (MDZ) was used as the target emerging contaminant and was sourced from Sigma Aldrich (USA). Copper sulphate pentahydrate (CuSO4.5H2O, BDH Chemical Ltd, England) served as the impregnating agent for adsorbent modification. Sodium chloride (NaCl) was used in the point of zero charge determination. All solutions were prepared with deionised water.

2.2 Preparation of Copper modified Snail Shell Biochar (SSB)

Shells of Lissachatina fulica were purchased from a local market in Warri, Delta State, Nigeria. They were soaked for three days, washed repeatedly with deionised water and a double-salt solution to remove slimy residues, and then sun-dried for five days. The dried shells were crushed with a laboratory mortar and pestle, further ground to powder using a dry hand grinder, and sieved through a

150 µm micro-sieve. The powder was pyrolysed in a muffle furnace at 700°C at a heating rate of 10°C/min for two hours, cooled to 30°C, and stored in a sealed container as the base adsorbent (SSB). Twenty grams of SSB was thoroughly mixed with 40 mL of a 0.5 M CuSO4 solution in a 1:2 mass-to-volume ratio. The mixture was stirred vigorously until a uniform slurry formed, allowed to stand for one hour, and then oven-dried at 60°C for three to five days. The resulting solid was pulverised, sieved through a 150 µm sieve, and stored in an airtight container, labelled Cu-SSB.

2.3 Characterisation of Cu-SSB

Surface morphology and elemental composition were examined by scanning electron microscopy coupled with energy-dispersive X-ray spectroscopy (SEM-EDX) using a Hitachi S4800 instrument (Japan), with powdered samples mounted on carbon tape-coated stubs. Crystalline phase identification was performed by X-ray diffraction (XRD) on a Rigaku Miniflex 600 instrument, with data processed using SMART LAB STUDIO II software and phases matched against a reference mineral database. Functional group characterisation was conducted by Fourier transform infrared spectroscopy (FTIR) using an IRTracer-100 spectrometer (Shimadzu, Japan). BET surface area, micropore diameter, and pore volume were determined from N2 adsorption-desorption isotherms. The pH of point of zero charge (pHpzc) was measured by a mass titration method in which 0.1 g of Cu-SSB was equilibrated in 50 mL of 0.5 M NaCl at pH values ranging from 2 to 12 on a shaker at 250 rpm for 24 hours, and the pHpzc was taken as the intersection of the final pH versus initial pH curve.

2.4 RSM Optimisation of MDZ Adsorption

Optimisation of MDZ removal on Cu-SSB was carried out using a Central Composite Design (CCD) within the Response Surface Methodology (RSM) framework, implemented in Design Expert software (version 13.0.5.0, Stat-Ease Inc., USA). Four independent variables were studied: pH (3 to 10), dosage (10 to 50 mg), contact time (20 to 120 min), and initial MDZ concentration (30 to 100 mg/L). The design was randomised with no blocking and produced 30 experimental runs, of which six were centre points, with percentage MDZ removal efficiency as the sole response variable. A reduced quadratic model was selected based on sequential model testing, with model adequacy assessed through analysis of variance (ANOVA), R2, adjusted R2, predicted R2, and the lack-of-fit test.

2.5 Adsorption Mechanisms

To understand the kinetics of the adsorption process contact time data for MDZ adsorption on Cu-SSB were fitted by nonlinear regression to three kinetic models: pseudo first order (PFO), pseudo second order (PSO), and Elovich. Model discrimination was based on the coefficient of determination (R^2), adjusted R^2, and root mean square error (RMSE). The Isotherm of the process was determined through Equilibrium concentration data for MDZ adsorption on Cu-SSB that were fitted by nonlinear regression to three isotherm models: Langmuir, Freundlich, and Temkin. Model selection was based on R^2, adjusted R^2, and reduced chi-square statistics.

3 RESULTS AND DISCUSSION

3.1 Physicochemical Characterization of Cu-SSB

Physicochemical characterisation of Cu-SSB was carried out using EDX, XRD, zeta potential measurement, FTIR spectroscopy, SEM imaging, and BET surface area analysis. The results collectively describe a crystalline, copper loaded composite with a chemically active surface whose properties vary predictably with pH.

BET analysis returned a specific surface area of 348.711 m2/g, a micropore diameter of 2.130 nm, and a BJH pore volume of 0.196 cc/g. The micropore diameter confirms nanosized pore presence within the matrix, consistent with the fine sub-micron copper features later visible in SEM. Copper sulphate impregnation introduces Cu particles into the biochar surface, which can enhance specific interactions with target contaminants (Quesada et al., 2021; Ali et al., 2024; Cui et al., 2024).

EDX analysis (Figure 1.1a) reveals a multi elemental surface composition following impregnation. Calcium remains the major component at 38.80 wt% (25.10 at%), though at a lower relative dominance than in unmodified SSB, reflecting the introduction of heavier elements. Tin appears at 23.11 wt% (5.05 at%), and copper at 8.04 keV (Ka) accounts for 22.32 wt% (9.12 at%), confirming successful incorporation. A prominent sulphur peak at 2.31 keV (8.56 wt%) indicates that the copper precursor was sulphate-based, an inference directly supported by the FTIR band at 1085 cm-1 attributed to surface rearrangement from sulphate interaction (Dahunsi et al., 2021). Potassium is also detected at 3.17 wt%, with trace iron, zinc, and silver. Taken together, the copper and sulphur concentrations point to a

chemically active surface capable of both adsorptive and catalytic interactions with metronidazole and PFOA.

XRD analysis (Figure 1.1b) confirms high crystallinity, with calcite as the most intense phase. A distinct CuO peak at approximately 36.5 degrees 2-theta verifies that the sulphate precursor identified in EDX was thermally converted to crystalline copper oxide on the biochar surface. Quartz (SiO2) appears as a trace mineral consistent with snail shell composition (Adepitan et al., 2025), and periclase (MgO) likely reflects minor mineral content from preparation. A broad, low-intensity amorphous signal persisting across the diffractogram corresponds to the underlying biochar phase, the same matrix whose rigid plate morphology is preserved in SEM despite calcination.

phpzc profiling (Figure 1.1c) places the point of zero charge at pH 8.53, indicating an alkaline surface character arising from copper loading. Below this value the surface carries a net positive charge, favouring uptake of negatively charged contaminants such as PFOA; above it the surface becomes negative, making it more suited to positively charged species. This pH-dependent charge behaviour is consistent with reported effects of metal loading on surface charge (Li et al., 2025) and is directly relevant to selecting operating conditions across the two contaminant systems investigated here.

FTIR spectra of SSB and Cu-SSB (Figure 1.1d) show clear changes attributable to copper incorporation. The O-H stretching band shifts from 3643 cm-1 in SSB to a broader, red-shifted band at 3552 cm-1 in Cu-SSB, consistent with hydroxyl group involvement in bonding with copper species (Al-Ghouti and Al-Absi, 2020). Both materials retain the calcite asymmetric stretching band at 1382 cm-1, confirming that the calcite framework identified in XRD remains chemically intact. Cu-SSB additionally shows a peak at 1085 cm-1 assigned to C-O stretching or silicate-carbonate interactions arising from copper loading (Dahunsi et al., 2021), which aligns with the sulphur concentration detected in EDX. A new band at 659 cm-1 is assigned to Cu-O stretching, independently corroborating the CuO phase identified in XRD (IISTE, 2020). The CO3(2-) bending bands at 865 cm-1 and 710 cm-1 remain intact across both materials, consistent with the calcite phase stability observed diffractometrically. Together, these spectral changes confirm successful copper loading and an increase in metal active sites and oxygen-containing functional groups relevant to contaminant removal (Agbale et al., 2024).

SEM imaging (Figure 1.2) shows numerous bright, granular deposits scattered across the irregular biochar surface, attributable to the crystalline CuO phases confirmed in XRD (Dahunsi et al., 2021). The underlying biochar retains its rigid, sharp-edged plate morphology, confirming structural survival through both impregnation and calcination. Interstitial voids and surface fissures remain visible throughout, maintaining the multiscale porosity consistent with the BET pore volume and micropore diameter recorded above (Agbale et al., 2024). Fragment sizes span from large support flakes exceeding 50 μm down to fine sub-micron metallic features, with the latter contributing disproportionately to the reactive surface area available for adsorption (IISTE, 2020). Some clustering of copper-rich particles is observed on the biochar surface, though dispersion across the composite remains broad (Al-Ghouti and Al-Absi, 2020).

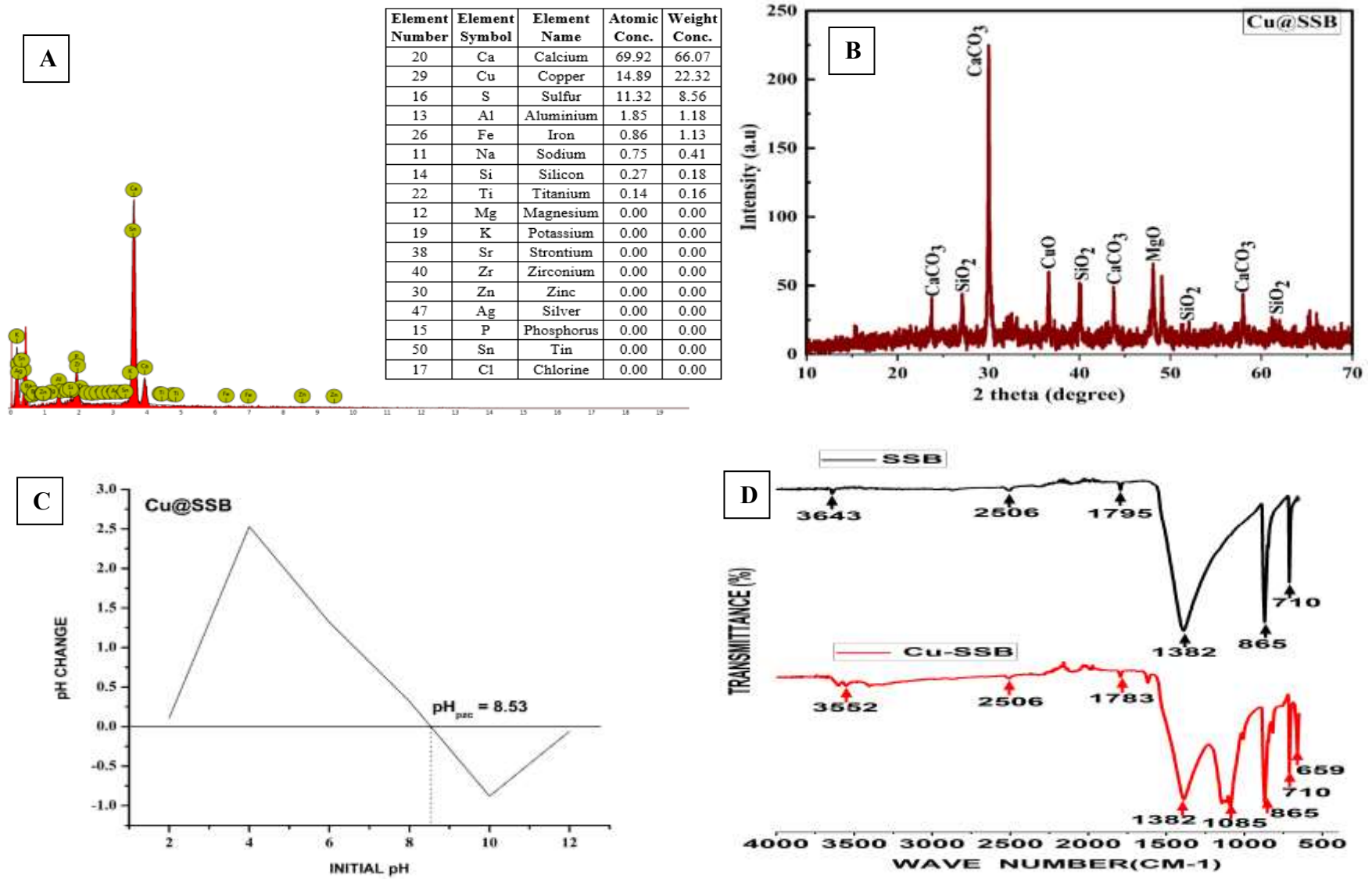

Element Number	Element Symbol	Element Name	Atomic Conc.	Weight Conc.
20	Ca	Calcium	69.92	66.07
29	Cu	Copper	14.89	22.32
16	S	Sulfur	11.32	8.56
13	Al	Aluminium	1.85	1.18
26	Fe	Iron	0.86	1.13
11	Na	Sodium	0.75	0.41
14	Si	Silicon	0.27	0.18
22	Ti	Titanium	0.14	0.16
12	Mg	Magnesium	0.00	0.00
19	K	Potassium	0.00	0.00
38	Sr	Strontium	0.00	0.00
40	Zr	Zirconium	0.00	0.00
30	Zn	Zinc	0.00	0.00
47	Ag	Silver	0.00	0.00
15	P	Phosphorus	0.00	0.00
50	Sn	Tin	0.00	0.00
17	Cl	Chlorine	0.00	0.00

Figure 1.1: Characterization of Cu-SSB: (a) EDX spectrum with elemental composition table; (b) XRD diffractogram; (c) pHpzc plot; (d) FTIR spectra showing a comparison between SSB and Cu-SSB.

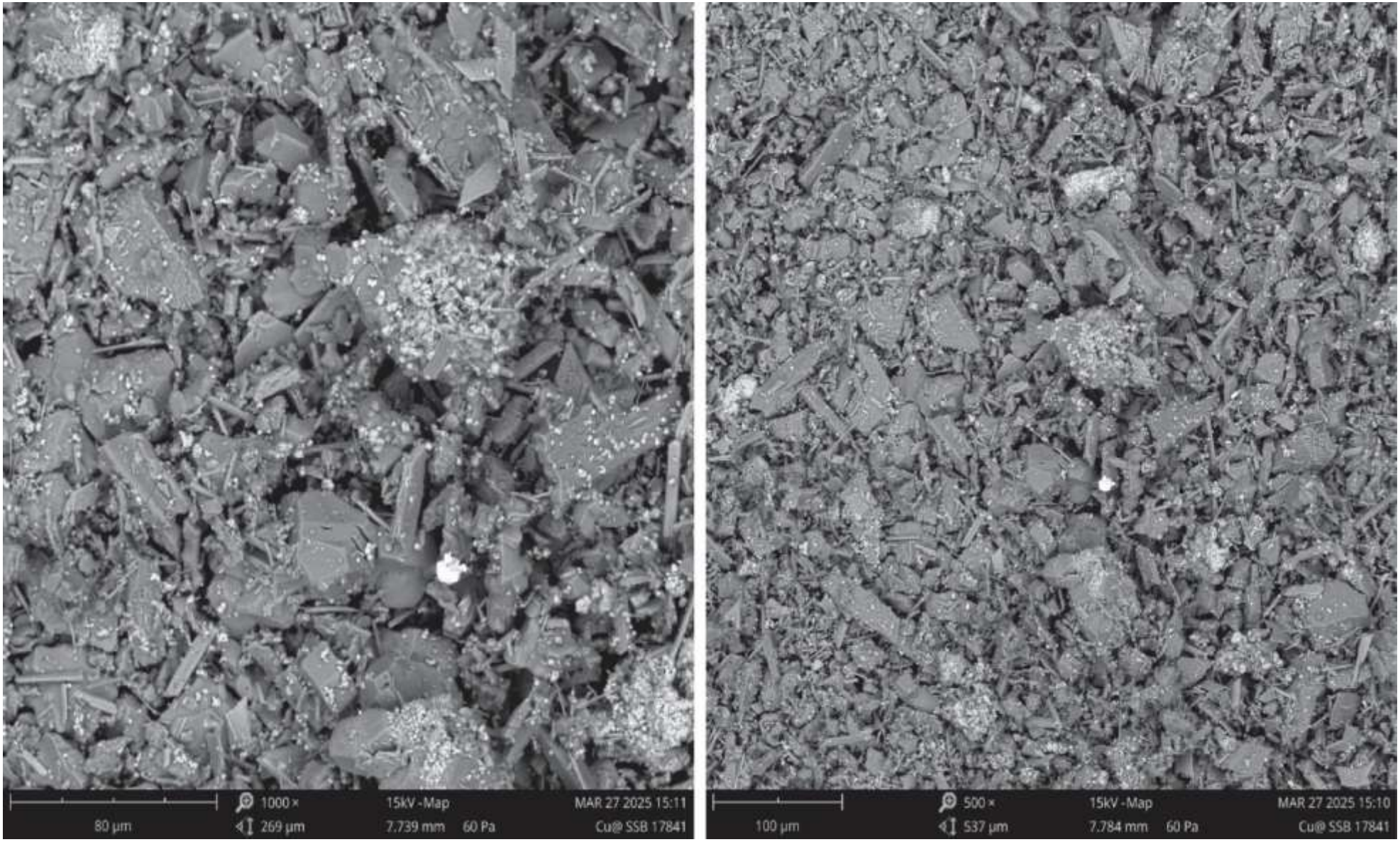

Figure 1.2: Scanning Electron Microscopy of Cu-SSB

3.2. Response Surface Method (RSM) Optimization Results

For this study, a Central Composite Design (CCD) was applied to model metronidazole removal using Cu-SSB, with four independent variables: pH (3 to 10), dosage (10 to 50 mg), contact time (20 to 120 min), and initial concentration (30 to 100 mg/L). The design, executed in Design Expert v13.0.5.0 under a randomized subtype with no blocks, produced 30 experimental runs comprising 24 non-centre points and 6 centre points. Factor ranges and coded levels are summarised in Table 1.

Table 1: Experimental building block in terms of coded and actual variables

Factor	Name	Units	Type	Subtype	Minimum	Maximum	Coded Low	Coded High	Mean	Std. Dev.
A	pH		Numeric	Continuous	3	10	-1 ↔ 1.00	+1 ↔ 10.00	6.8	2.26
B	Dosage	Mg	Numeric	Continuous	10	50	-1 ↔ 10.00	+1 ↔ 50.00	30	12.86
C	Time	Min	Numeric	Continuous	20	120	-1 ↔ 20.00	+1 ↔ 120.00	64.33	32.55
D	Initial Conc.	mg/L	Numeric	Continuous	30	100	-1 ↔ 30.00	+1 ↔ 100.00	56	23.72

Sequential model fitting (Table 2) guided model selection. The linear model was statistically significant ($p = 0.0018$) but its adjusted R^2 (0.4012) and predicted R^2 (0.2280) differed by more than 0.2, indicating that first-order terms alone could not capture the complexity of the system. The quadratic model improved fit substantially ($p = 0.0005$, adjusted $R^2 = 0.8089$, predicted $R^2 = 0.6426$), and a non-significant lack of fit ($p = 0.9604$) confirmed agreement with the observed data.

Table 2: Sequential Model Sum of Squares CU-SSB Performance

Source	Sum of Squares	df	Mean Square	F-value	p-value	
Mean vs Total	74400.10	1	74400.10			
Linear vs Mean	13382.57	4	3345.64	5.86	0.0018	
2FI vs Linear	4738.92	6	789.82	1.57	0.2091	
Quadratic vs 2FI	6805.84	4	1701.46	9.34	0.0005	Suggested
Cubic vs Quadratic	681.52	9	75.72	0.2214	0.9781	Aliased
Residual	2052.22	6	342.04			
Total	1.021E+05	30	3402.04			

ANOVA for the reduced quadratic model (Table 3) returned an F-value of 13.38 ($p < 0.0001$), confirming model significance. The R^2 of 0.8910 indicates that 89.10% of response variability is explained by the selected factors and their interactions. The difference between R^2 and adjusted R^2 (0.8244) is 0.0666, ruling out term inflation. A non-significant lack of fit ($p = 0.9723$) further confirms that the quadratic surface adequately represents the system.

Table 3: ANOVA for Reduced Quadratic model CU-SSB Performance

Source	Sum of Squares	df	Mean Square	F-value	p-value	
Model	24646.65	11	2240.60	13.38	< 0.0001	significant
A-pH	2317.02	1	2317.02	13.84	0.0016	
B-Dosage	6078.77	1	6078.77	36.30	< 0.0001	
C-Time	1191.79	1	1191.79	7.12	0.0157	
D-Initial Conc	4982.57	1	4982.57	29.75	< 0.0001	
AB	2464.77	1	2464.77	14.72	0.0012	
AD	575.87	1	575.87	3.44	0.0801	
BC	1024.05	1	1024.05	6.11	0.0236	
CD	420.84	1	420.84	2.51	0.1303	
B^2	1920.03	1	1920.03	11.47	0.0033	
C^2	2481.27	1	2481.27	14.82	0.0012	
D^2	1856.30	1	1856.30	11.08	0.0037	
Residual	3014.40	18	167.47			
Lack of Fit	*1253.50*	*13*	*96.42*	*0.2738*	*0.9723*	*not significant*
Pure Error	1760.90	5	352.18			

Cor Total	27661.06	29

Among the linear terms, dosage (B) exhibited the most pronounced effect (SS = 6,078.77, F-value = 36.30, p-value < 0.0001) this shows that adsorbent dosage has the strongest individual influence on Cu-SSB performance. Initial concentration of metronidazole (D) also demonstrated a highly significant effect (SS = 4,982.57, F-value = 29.75, p-value < 0.0001), suggesting that the starting concentration significantly impacts the adsorption process. pH (A) showed a sum of squares of 2,317.02 (F-value = 13.84, p-value = 0.0016). Contact time (C) had the smallest but still significant effect among the linear terms (SS = 1,191.79, F-value = 7.12, p-value = 0.0157), indicating that the duration of contact between adsorbent and adsorbate influences equilibrium attainment.

Several two factor interaction terms were statistically significant. The interaction between pH and dosage (AB) was highly significant (p-value = 0.0012), this was the same for dosage and time interaction (BC) (p-value = 0.0236), suggesting a combined influence of these variables on adsorption performance CU-SSB adsorption. In contrast, the interaction between time and initial concentration (CD) was not significant (p-value = 0.1303), similar to that between pH and initial concentration (AD) which approached significance (p-value = 0.0801), indicating that these factors are independent of each other within the studied range.

The quadratic terms for dosage (B^2), time (C^2), and initial concentration (D^2) were all highly significant (p-value = 0.0033, 0.0012, and 0.0037, respectively), with sum of squares values of 1,920.03, 2,481.27, and 1,856.30. The prominence of C^2 indicates a strong non linear dependence of adsorption on contact time, whereas the significant B^2 and D^2 terms suggest the existence of practical limits beyond which further increases in dosage or initial concentration yield diminishing improvements in performance.

The final model:

$$\mathbf{Cu-SSB_{Performance}}\ (\%) = -19.6024\,A + 27.3235\,B + 10.9509\,C - 24.2759\,D - 31.7029\,AB + 15.7916\,BC - 16.5802\,B^2 - 19.7956\,C^2 + 21.0036\,D^2 + 54.1298$$

The reduced quadratic model is statistically valid and adequate for describing Cu-SSB adsorption, confirmed not just by the high R^2 value (0.8910) and F-value (13.38, $p < 0.0001$), but also by a not significant lack of fit ($p = 0.9723$), this provides confidence that the reduced quadratic model is appropriate for the system under study and that the curvature in the response surface is adequately captured by the quadratic terms. Based on the models' central composite design identified optimal adsorption conditions at pH 1, dosage 39.53 mg, contact time 35.09 min, and initial metronidazole concentration 30.34 mg/L. Under these conditions, removal efficiencies reached 99% for Cu-SSB,

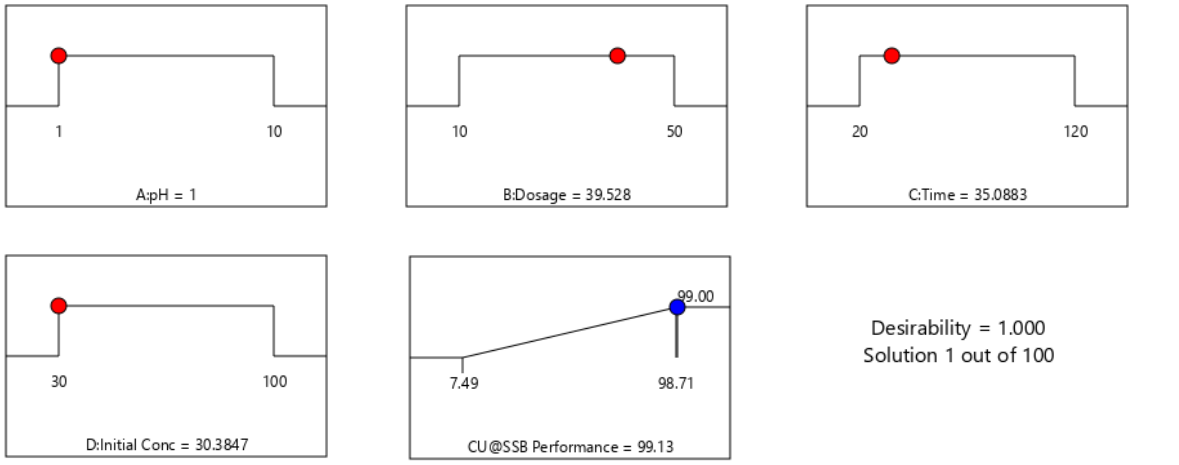

Figure 3: Removal efficiency at Optimum Conditions.

Table 4: Result of RSM experimental matrix including adsorbent performance and model prediction

Run	A:pH	B:Dosage (Mg)	C:Time (Min)	D:Initial Conc (mg/L)	CU-SSB Performance (%)	
					Actual	Predicted
1	7	30	20	30	49.84	57.40
2	10	30	20	50	23.452	20.15
3	3	50	60	50	98.452	97.23
4	7	10	70	100	7.486	6.17
5	3	30	120	50	61.582	71.09
6	7	10	20	50	15.614	11.54
7	3	30	20	50	50.258	41.00
8	7	30	20	100	11.405	18.31
9	7	50	120	50	82.774	75.14
10	10	10	60	50	35.356	42.15
11	10	30	120	50	43.582	50.24
12	10	30	60	30	96.613	89.38
13	7	10	120	50	21.518	10.05
14	7	10	60	30	54.677	62.63
15	7	30	120	30	98.227	98.41
16	7	30	120	100	18.227	21.10
17	7	50	20	50	11.454	13.47
18	7	50	60	30	98.71	89.82
19	10	50	60	50	24.742	27.07
20	7	30	60	50	52.872	60.12
21	3	10	60	50	11.55	13.68
22	7	30	60	50	55.388	60.12
23	10	30	60	100	29.544	15.72
24	7	30	60	50	82.066	60.12
25	7	30	60	50	78.322	60.12
26	7	50	60	100	22.05	35.45
27	7	30	60	50	53.356	60.12
28	7	30	60	50	31.194	60.12
29	3	30	60	30	96.937	97.37
30	3	30	60	100	76.741	68.71

3.3 Analysis of Cu-SSB Surface plots

This performance reached an impressive optimum of 99.13%, the highest of all the systems studied using response surface methodology. Performance was consistently high only in the low pH region in Plots 1, 2, and 3, where pH was paired with dosage, time, and initial concentration, respectively, under fixed conditions. As pH increased, performance collapsed sharply regardless of what the paired variable was doing. This behaviour supports the idea that pH is a significant main effect (F-value = 13.84, p = 0.0016).

The significant AB interaction (p = 0.0012) was well reflected in Plot 1, where high dosage at low pH produced the sharpest performance peak, indicating that dosage amplifies the benefit of acidic conditions rather than acting independently. Plot 2 showed that time has a secondary but meaningful role at low pH, consistent with its significance as a main effect (p = 0.0157), though performance remained broadly elevated across most of the time range when pH was already optimal. Plots 4, 5, and 6, all evaluated at fixed low pH, revealed the behaviour of the remaining variables under ideal acidity. The BC interaction (p = 0.0236) was apparent in Plot 16, where dosage and time needed to increase together to drive performance upward, confirming their synergistic relationship.

Plot 4 showed a similarly positive interaction between dosage and initial concentration, supported by the significance of both B^2 (p = 0.0033) and D^2 (p = 0.0037), which suggest that neither variable improves performance indefinitely. Plot 6 demonstrated that once pH and dosage are fixed at optimal levels, the system becomes largely insensitive to variations in time and concentration, a finding that reflects the not linear time dependence captured by the significant C^2 term (p = 0.0012).

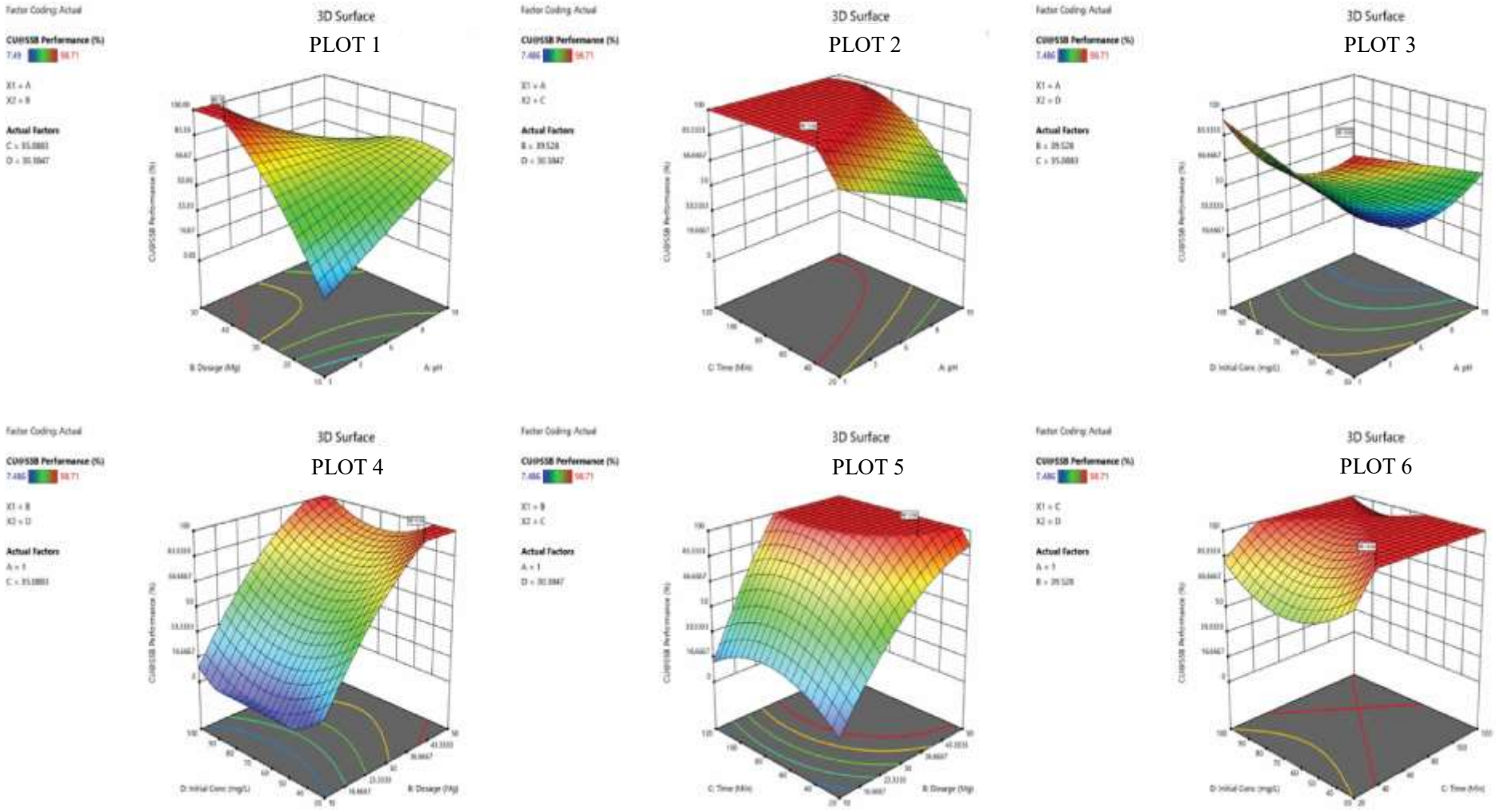

Figure 4: Cu-SSB Surface Plots: Plot 1. A (pH) vs. B (Dosage); Plot 2. A (pH) vs. C (Time); Plot 3. A (pH) vs. D (Initial Concentration); Plot 4. B (Dosage) vs. C (Time); Plot 5. B (Dosage) vs. D (Initial Concentration); Plot 6. C (Time) vs. D (Initial Concentration).

3.4 Isotherm of MDZ Adsorption onto Cu-SSB

Table 5 summarises the kinetic model fitting results for Cu-SSB in the adsorption of metronidazole. The PFO model gave an equilibrium adsorption capacity of 9.089 mg/g and a rate constant of 1.361×10^{-2} min^{-1}, with an R^2 of 0.8320 and a RMSE of 2.068. The PSO model returned an equilibrium adsorption capacity of 10.378 mg/g and a rate constant of 1.66×10^{-3} L mg^{-1} min^{-1}, but with an R^2 of 0.7972 and a RMSE of 2.496, lower than the PFO fit. The Elovich model fit gave a = 0.325 mg/g·min and b = 0.447 g/mg, with an R^2 of only 0.7445. This is the weakest Elovich fit across all adsorbent systems examined, and the relatively high b value indicates fast site deactivation, possibly reflecting a limited number of accessible binding sites on the Cu-SSB surface or a more homogeneous surface that the Elovich framework is poorly suited to describe. (Fouad *et al*., 2024)

Table 5: Cu-SSB adsorption kinetic parameters

Parameters	Pseudo First Order	Pseudo Second Order	Elovich Model
Qe	9.08919 ± 0.56889	10.37836 ± 0.99929	-
K	0.01361 ± 0.0032	0.00166 ± 7.69186E-4	-
A	-	-	0.32455 ± 0.20146
B	-	-	0.44735 ± 0.10939
RMSE	2.06792	2.496	3.1448
R^2	0.83196	0.79718	0.74446
Adj. R^2	0.82076	0.78366	0.72742

3.5 Isotherm Analysis of MDZ Adsorption for Cu-SSB

From Table 6, the Langmuir model best describes MDZ adsorption onto Cu-SSB, with R^2 = 0.9823 and a reduced chi-square of 0.200, outperforming Freundlich (R^2 = 0.9775, reduced chi-square = 0.106) despite the latter's lower absolute error. The Langmuir q_m of 11.93 mg/g is more than double that of K-SSB (5.33 mg/g), pointing to the role of Cu^{2+} ions in generating a denser population of discrete, high affinity binding sites across the biochar surface. The K_L value of 0.011 L/mg is comparable to K-SSB, suggesting that while Cu modification significantly increased site density (q_m), the binding strength per site at low concentration is similar. The Freundlich K_f of 0.669, over four times that of K-SSB, confirms substantially greater adsorption capacity under the tested conditions, while n = 2.13 reflects moderate surface heterogeneity. The Langmuir preference over Freundlich indicates that at saturation, adsorption converges toward a finite monolayer limit rather than continuing to grow across multiple energetically distinct layers. The Temkin model is the weakest fit (R^2 = 0.9520, reduced chi-square = 0.257); the qt of 2.235 J/mol and K_t of 0.171 L/g suggest weak average binding energy, inconsistent with the strong site-specific interactions implied by the Langmuir dominance.

Table 6: Isotherm Parameters for Cu-SSB

Parameter	Langmuir Model	Freundlich Model	Temkin Model
Equation	qm·KL·Ce / (1 + KL·Ce)	Kf·Ce^(1/n)	qt·ln(Kt·Ce)
Qm	11.930 ± 0.837		
Kf		0.669 ± 0.010	
Qt			2.235 ± 0.016
KL	0.011 ± 0.002		
N		2.128 ± 0.014	
Kt			0.171 ± 0.004
Reduced Chi-Sqr	0.19988	0.10631	0.25731
RSS	1.59904	106.09746	256.79066
R^2	0.98231	0.97753	0.95198
Adj. R^2	0.98010	0.97750	0.95193

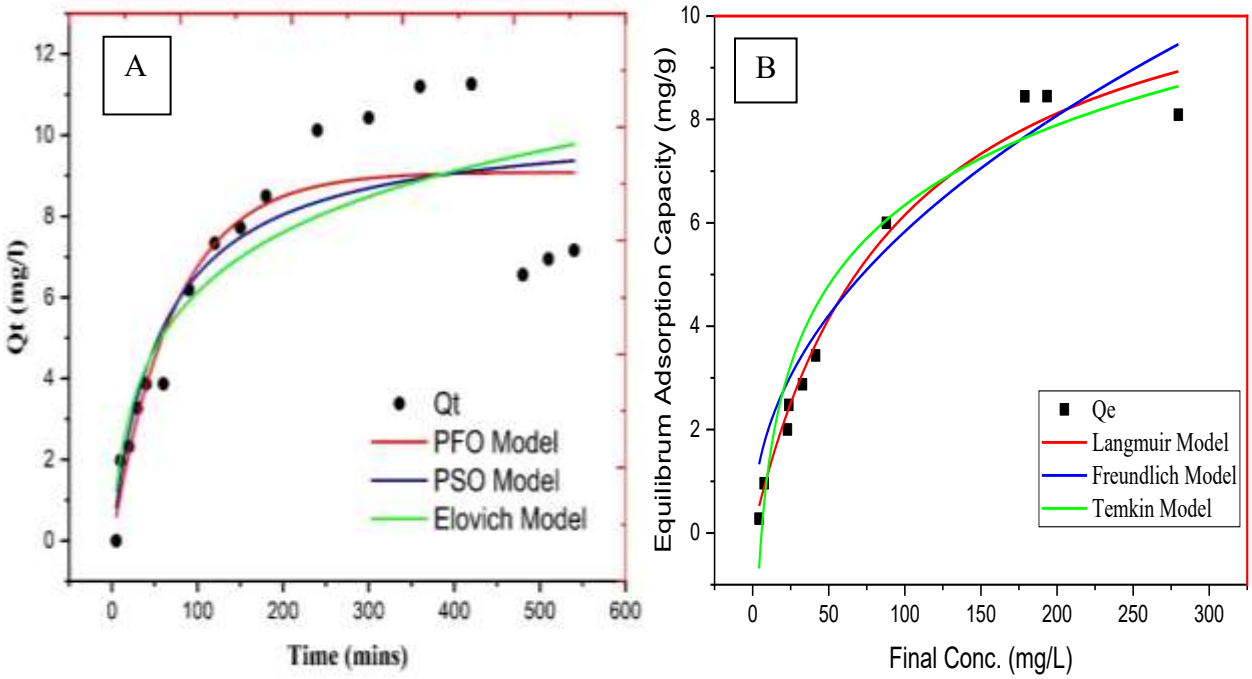

Figure 5: **(A)** Adsorption Kinetic plots with Pseudo First Order, Pseudo Second Order and Elovich fittings of *Cu-SSB* **(B)** Graph of Equilibrium adsorption capacity (qe) vs Final Concentration (Ce) for *Cu-SSB*

Table 7: Effect of time on MDZ adsorption at PH =7, Dosage =50mg, initial conc.=30mg/L, and volume = 20ml at 25°C; for Kinetics assessment

Time (mins)	Co (mg/L)	Ce (mg/L)	Qt (mg/g)
5.00	30	29.9990	0.00
10.00	30	25.0640	1.97
20.00	30	24.1930	2.32
30.00	30	21.8220	3.27
40.00	30	20.3220	3.87
60.00	30	17.3220	3.87
90.00	30	14.5160	6.19
120.00	30	11.6610	7.34
150.00	30	10.6930	7.72
180.00	30	8.7580	8.50
240.00	30	4.6930	10.12
300.00	30	3.9190	10.43
360.00	30	1.9840	11.21
420.00	**30**	**1.8390**	**11.26**
480.00	30	13.5990	6.56
510.00	30	12.6290	6.95
540.00	30	12.0970	7.16

Table 8: Effect of temperature on MDZ adsorption at PH =7, Dosage =50mg, and volume = 20ml at 25°C, for isotherm analysis

Dosage (g)	Volume (ml)	Co(mg/L)	Ce(mg/L)	Qe(mg/g)
0.05	0.02	5	4.306	0.2776
0.05	0.02	10	7.597	0.9612
0.05	0.02	20	22.919	2
0.05	0.02	30	23.806	2.4776
0.05	0.02	40	32.806	2.8776
0.05	0.02	50	41.419	3.4324
0.05	0.02	100	87.918	6
0.05	0.02	200	178.884	8.4464
0.05	0.02	250	193.499	8.45
0.05	0.02	300	279.769	8.0924

4 CONLUSION

4.1 Summary of Findings

- Copper modified snail shell biochar (Cu-SSB) was successfully synthesised from *Lissachatina fulica* shells through pyrolysis at 700°C followed by $CuSO_4$ impregnation. Physicochemical characterisation confirmed a high specific surface area of 348.71 m^2/g, crystalline CuO phases on the biochar matrix, and a point of zero charge at pH 8.53, collectively indicating a chemically active surface well-suited for contaminant uptake. FTIR and XRD analyses verified successful copper incorporation, evidenced by the emergence of a Cu–O stretching band at 659 cm^{-1} and a distinct CuO diffraction peak, while SEM imaging revealed preserved porosity and broadly dispersed copper-rich deposits across the adsorbent surface.
- Response surface methodology, implemented through a Central Composite Design, identified optimal MDZ removal conditions at pH 1, a dosage of 39.53 mg, a contact time of 35.09 min, and an initial concentration of 30.34 mg/L, achieving a removal efficiency of 99%. The reduced quadratic model demonstrated strong predictive reliability ($R^2 = 0.8910$, $p < 0.0001$), with adsorbent dosage and initial contaminant concentration emerging as the most influential process variables. Significant interaction effects between pH and dosage, and between dosage and contact time, revealed that acidic conditions amplify the benefit of increased adsorbent loading rather than acting independently.
- Equilibrium data were best described by the Langmuir isotherm model ($R^2 = 0.9823$, qm = 11.93 mg/g), confirming monolayer adsorption onto a finite number of discrete binding sites generated by copper modification. Kinetic fitting favoured the pseudo-first-order model ($R^2 = 0.8320$), suggesting that the rate of MDZ uptake is primarily governed by the available surface concentration of active sites rather than by bimolecular surface reactions.

4.2 Conclusion

The results demonstrate that copper modification of snail shell biochar substantially enhances its capacity for metronidazole removal, producing a material whose adsorption performance is governed by site specific physiosorptive interactions consistent with Langmuir monolayer behaviour. Unlike conventional treatment approaches that rely on costly synthetic adsorbents, Cu-SSB valorises abundant agricultural waste into a high-performance remediation material, closing a meaningful gap between laboratory-scale innovation and economically accessible water treatment technology. The RSM-optimised framework further establishes that near-complete MDZ elimination is achievable under carefully controlled acidic conditions, with process variables interacting in ways that single-factor experiments would fail to capture. These findings carry direct relevance for water treatment practice in regions where pharmaceutical contamination of surface and groundwater is an escalating public health concern. The material's straightforward synthesis from locally available biomass feedstock positions it as a scalable candidate for adoption in decentralised treatment systems, small municipal facilities, and industrial effluent management operations across West Africa, where both the raw material supply and the remediation need are substantial.

4.3 Recommendations for Future Studies

- While this study establishes Cu-SSB as a high-efficiency adsorbent under controlled batch conditions, several dimensions of its performance remain uncharacterised and warrant systematic investigation. The optimal pH of 1 identified by the RSM model, though statistically derived, falls outside the pH range tested experimentally; future work should validate this prediction through targeted experiments and explore the practical feasibility of operating at extreme acidity in real treatment scenarios.
- Adsorbent regeneration and reusability across multiple adsorption–desorption cycles have not been evaluated and represent a critical gap for any commercial application claim. Studies employing mild thermal or chemical desorption protocols would establish whether Cu-SSB can operate within a circular economy framework without significant loss of capacity. Additionally, performance should be assessed in authentic wastewater matrices containing competing ions, natural organic matter, and co-occurring contaminants, as the controlled single-solute conditions used here may overestimate removal efficiency in field applications.
- Finally, pilot scale continuous flow column studies are needed to translate the batch adsorption parameters established in this work into design criteria applicable to operational water treatment infrastructure. Thermodynamic profiling across a broader temperature range would further clarify the energetics of MDZ binding and strengthen the mechanistic interpretation of the adsorption process.

REFERENCES

Abdi, J., Firozjaee, T. T., Mohammadian, N., & Jalalian, H. (2025). Sustainable technologies for the remediation of metronidazole antibiotic from aqueous solution: Current and future perspectives. Results in Chemistry. https://doi.org/10.1016/j.rechem.2025.102439

Adepitan, O. L., Alabi, O. O., Gbadeyan, O. J., Deenadayalu, N., & Jayeola, A. T. (2025). Investigation into the development and utilization of snail shell biomaterials: a systematic review. Discover Materials, 5(1).

Agbale, N. R., Adeniyi, O. D., & Abdulkareem, A. S. (2024). Assessment of engineered snail shell - plantain pseudo stem biochar composite for remediation. Nigerian Journal of Engineering, 31(1), 31-44.

Al-Ghouti, M. A., & Al-Absi, R. S. (2020). FTIR Spectroscopic Analysis of Snail Shells. Scientific Reports.

Ali Babeker, T. M., Lv, S., Wu, J., Zhou, J., & Chen, Q. (2024). Insight into Cu (II) adsorption on pyrochar and hydrochar resultant from Acacia Senegal waste for wastewater decontamination. Chemosphere, 356, 141881. https://doi.org/10.1016/j.chemosphere.2024.141881

Chebbi, M., Ounoki, S., Youcef, L., & Amrane, A. (2023). Synthesis and characterization of pine cones biochar for the removal of an antibiotic (metronidazole) from aqueous solutions. Journal of Industrial & Engineering Chemistry. https://doi.org/10.1016/j.jiec.2023.06.023

Cui, Z., Wang, Y., Wang, N., Ma, F., & Yuan, Y. (2024). Effects of Ageing on Surface Properties of Biochar and Bioavailability of Heavy Metals in Soil. Agriculture, 14(9). https://doi.org/10.3390/agriculture14091631

Dahunsi, O., Oyehan, T. A., & Oyewole, O. A. (2021). Development of snail shell biochar for the removal of pharmaceuticals from wastewater. Environmental Technology & Innovation.

Diwan, V., Tamhankar, A., Aggarwal, M., Sen, S., Khandal, R. K., & Lundborg, C. (2009). Detection of antibiotics in hospital effluents in India. Current Science.

Fouad, Mohamed & El-Aswad, Ahmed & Aly, Maher. (2024). Mathematical models of the adsorption-desorption kinetics of fenitrothion in clay soil and sandy clay loam soil. Current Chemistry Letters. 13. 641-654. 10.5267/j.ccl.2024.6.002.

Ighalo, J. O., Igwegbe, C., Adeniyi, A., Adeyanju, C., & Ogunniyi, S. (2020). Mitigation of metronidazole (Flagyl) pollution in aqueous media by adsorption: A review. Environmental Technology Reviews. https://doi.org/10.1080/21622515.2020.1849409

IISTE. (2020). Chemical and Phase Characterization of Snail Shell Particles. Chemistry and Materials Research, 12(6).

Jia, Y., Ou, Y., Khanal, S., Sun, L., Shu, W.-S., & Lu, H. (2024). Biochar-based strategies for antibiotics removal: Mechanisms, factors, and application. ACS ES&T Engineering. https://doi.org/10.1021/acsestengg.3c00605

Jiang, C., Yue, F., Li, C., Zhou, S., & Zheng, L. (2022). Polyethyleneimine-modified lobster shell biochar for the efficient removal of copper ions in aqueous solution: Response surface method optimization and adsorption mechanism. Journal of Environmental Chemical Engineering. https://doi.org/10.1016/j.jece.2022.108996

Lanzky, P. F., & Halling-Sørensen, B. (1997). The toxic effect of the antibiotic metronidazole on aquatic organisms. Chemosphere. https://doi.org/10.1016/S0045-6535(97)00324-X

Li, Y., Zhao, B. & Shang, T. Adsorption of copper(II) in biochar-humic acid–water system. Sci Rep 15, 24948 (2025). https://doi.org/10.1038/s41598-025-09880-5

Majidi, S., Pourzamani, H., & Ebrahimpour, K. (2024). Estimating release of the antibiotic metronidazole into the environment from hospital effluents and assessment of the associated ecological risk: A case study in Isfahan, Iran (2023). Human and Ecological Risk Assessment. https://doi.org/10.1080/10807039.2024.2399695

Quesada, H. B., De Araújo, T. P., Cusioli, L. F., De Barros, M. A. S. D., Gomes, R. G., & Bergamasco, R. (2021). Evaluation of novel activated carbons from chichá-do-cerrado (Sterculia striata St. Hil. Et Naud) fruit shells on metformin adsorption and treatment of a synthetic mixture. Journal of Environmental Chemical Engineering, 9(1), 104914. https://doi.org/10.1016/j.jece.2020.104914

Ren, H., Ma, X., Ma, B., Bai, X., Wang, H., Ma, Z., Gu, S., & Wang, J. (2025). DFT-validated adsorption mechanisms of metronidazole on CO_2-activated almond shell biochar for antibiotic wastewater treatment. Desalination and Water Treatment. https://doi.org/10.1016/j.dwt.2025.101414

Sen, U., Esteves, B., Aguiar, T., & Pereira, H. (2023). Removal of antibiotics by biochars: A critical review. Applied Sciences, 13(21), 11963. https://doi.org/10.3390/app132111963

Sophia, C. A., & Lima, E. (2018). Removal of emerging contaminants from the environment by adsorption. Ecotoxicology and Environmental Safety. https://doi.org/10.1016/j.ecoenv.2017.12.026